

**DEVELOPMENT OF LAB ON PRINTED CIRCUIT  
BOARD BASED HEAVY METAL DETECTION**

**BEH KHI KHIM**

**UNIVERSITI SAINS MALAYSIA**

**2023**

# **DEVELOPMENT OF LAB ON PRINTED CIRCUIT BOARD BASED HEAVY METAL DETECTION**

by

**BEH KHI KHIM**

**Thesis submitted in fulfilment of the requirements  
for the degree of  
Doctor of Philosophy**

**May 2023**

## ACKNOWLEDGEMENT

First and foremost, I would like to thank my supervisor, Associate Professor Dr. Asrulnizam bin Abd Manaf. Throughout my PhD journey, he has been a tremendous source of support and invaluable guidance. He has always impressed me with his impeccable professional conduct and unwavering belief in science, technology, and the future. Our meetings were highly beneficial, and he assisted me in all aspects of my work and life philosophy. Aside from that, I'd like to thank Associate Professor Dr. Oo Chuan Wei, my co-supervisor from School of Chemical Sciences for guiding me through heavy metals.

Working with everyone from the USM Engineering Campus to the USM Main Campus has been a pleasure. I want to express my heartfelt gratitude to Dr. Beh Khi Poay and Dr. Yam Fong Kwong from the School of Physics in particular, for their unwavering support of my work. I am also grateful to all of the CEDEC research officers and technical staff, particularly Miss Sofiyah Binti Sal Hamid, Mr. Khairu Anuar Bin Mohamed Zain, Mr. Abdullah Sanusi Bin Husain, and Mr. Aminudin Bin Mustafa, for their technical assistance and courage while conducting my experiments. Next, I'd like to thank my family, particularly my parents, who have worked tirelessly to raise and educate me to this day.

Furthermore, I would like to thank University Sains Malaysia for funding my research through the Top-Down Research University (USM) grant number 1001/PCEDEC/870050 and Professor Kazuaki Sawada of Toyohashi University of Technology.

Finally, I'd like to take this opportunity to remind all future me to remain humble, honest, and self-disciplined. This thesis, however, was completed in the post-pandemic

era of Covid-19. Remember to love yourself and those around you, especially your family and loved ones.

## TABLE OF CONTENTS

<b>ACKNOWLEDGEMENT</b> .....	<b>ii</b>
<b>TABLE OF CONTENTS</b> .....	<b>iv</b>
<b>LIST OF TABLES</b> .....	<b>ix</b>
<b>LIST OF FIGURES</b> .....	<b>xi</b>
<b>LIST OF SYMBOLS</b> .....	<b>xviii</b>
<b>LIST OF ABBREVIATIONS</b> .....	<b>xx</b>
<b>ABSTRAK</b> .....	<b>xxiii</b>
<b>ABSTRACT</b> .....	<b>xxv</b>
<b>CHAPTER 1 INTRODUCTION</b> .....	<b>1</b>
1.1 Overview .....	1
1.2 Heavy Metal Pollutions in Malaysia .....	2
1.3 Problem Statement .....	4
1.4 Research Objective.....	5
1.5 Research Scope and Limitation.....	6
1.6 Organization of Thesis .....	6
<b>CHAPTER 2 LITERATURE REVIEW</b> .....	<b>8</b>
2.1 Overview .....	8
2.2 Heavy Metal Exposure .....	8
2.3 Heavy Metal Sensor .....	11
2.3.1 Colorimetric sensing .....	12
2.3.2 Magnetic relaxation sensor.....	14
2.3.3 Optical Fiber Sensor.....	15
2.3.4 Electrochemical Sensor .....	15
2.3.4(a) Potentiostatic technique .....	19
2.3.4(b) Amperometry .....	20

	2.3.4(c) Chronocoulometry .....	20
	2.3.4(d) Voltammetric techniques .....	21
	2.3.5 Heavy Metal Sensor summary .....	30
2.4	Heavy Metal Sensor Design .....	31
	2.4.1 Form factor .....	32
	2.4.1(a) Sensor Electrode's Form factor .....	34
	2.4.2 General Theories .....	35
	2.4.3 Electrode Materials .....	36
2.5	Heavy Metal Sensor Substrate .....	36
	2.5.1 Ceramic substrate .....	37
	2.5.2 Paper based substrate .....	38
	2.5.3 PDMS substrate.....	39
	2.5.4 Glass substrate.....	39
	2.5.5 Silicon substrate .....	40
	2.5.6 PET substrate.....	41
	2.5.7 FR-4 substrate .....	41
	2.5.8 Comparison of substrates .....	42
2.6	Electroplating .....	43
	2.6.1 Active and Inert Electrodes .....	44
2.7	Sensor Modification .....	46
2.8	Graphene Oxide.....	47
	2.8.1 Graphite Oxidation Methods.....	49
	2.8.1(a) Brodie Method .....	50
	2.8.1(b) Staudenmaier Method.....	50
	2.8.1(c) Hummer Method.....	51
	2.8.1(d) Tour Method .....	52
	2.8.2 Graphite Oxidation Summary .....	53

2.9	Microfluidic Device .....	54
2.10	Characterizations .....	55
2.10.1	Potentiostat .....	55
2.10.2	Field Emission Scanning Electron Microscope (FESEM) and Energy Dispersive X-rays (EDX) .....	57
2.10.3	Transmission Electron Microscope (TEM).....	60
2.10.4	High Resolution X-ray Diffraction (HR-XRD) .....	62
2.10.5	Ultraviolet–visible spectroscopy .....	65
2.10.6	Fourier transform infrared spectroscopy .....	66
2.10.7	Raman spectroscopy.....	67
2.11	Summary .....	69
<b>CHAPTER 3 METHODOLOGY.....</b>		<b>71</b>
3.1	Introduction .....	71
3.2	Sensing Principles and EC Sensor Design Structure.....	73
3.2.1	Sensing Principles .....	73
3.3	EC Sensor Design Structure .....	75
3.4	Current response of the sensor .....	77
3.5	Ohmic drop across the sensor.....	79
3.6	Sensor Design Summary .....	81
3.7	EC Sensor Fabrication.....	82
3.8	Electroplating process for the EC Sensor.....	84
3.8.1	Calculation of Electroplating time .....	85
3.8.2	Overview of Nickel electroplating.....	87
3.8.3	Electroplating setup.....	88
3.9	Graphene Oxide Synthesis .....	90
3.9.1	Chemical and materials .....	90
3.9.2	Graphene Oxide synthesis procedure.....	90
3.10	Modification of EC Sensor.....	93

3.11	Microfluidic Device integration on EC Sensor .....	94
3.11.1	Microfluidic design for EC Sensor.....	95
3.11.2	Microfluidic fabrication for EC Sensor.....	95
3.12	Demonstration of lab on chip heavy metal sensor .....	98
3.13	Experiment Setup .....	99
3.13.1	First Component.....	100
3.13.2	Second Component .....	102
3.13.3	Third Component .....	103
3.14	Summary .....	104
<b>CHAPTER 4 RESULTS AND DISCUSSION.....</b>		<b>106</b>
4.1	Introduction .....	106
4.2	Graphite Flakes .....	106
4.3	Graphene Oxide.....	107
4.3.1	Morphological Studies of Graphene Oxide.....	107
4.3.1(a)	Effect of Graphene Oxide Concentration on Surface Roughness.....	109
4.3.2	UV Reflectance Analysis .....	113
4.3.3	Raman Spectroscopy Analysis.....	114
4.3.4	FTIR Spectroscopy Analysis.....	115
4.4	Design and Characterization of Electrochemical (EC) Sensor Design .....	117
4.4.1	Morphological Aspects of Electroplated Electrodes.....	117
4.4.2	Cross-sectional area of the EC sensor .....	121
4.4.3	Solid-state Silver/Silver Chloride reference electrode.....	122
4.5	Parametric Investigation of Printed Circuit Board based Electrochemical Sensor.....	124
4.5.1	Generation 1 EC sensor – highlights and flaws .....	125
4.5.1(a)	DOE Results for Generation 1 EC Sensor.....	126
4.5.2	Generation 2 EC sensor – highlights and flaws .....	128

	4.5.2(a) DOE Results for Generation 2 EC Sensor.....	130
4.6	Final design (Generation 3) EC Sensor.....	131
	4.6.1 Preliminary electrode assessment through Cyclic Voltammetry measurements .....	133
	4.6.2 CV measurement for EC sensor of various CE/WE size ratio.....	134
	4.6.3 CV measurement using PBS electrolyte .....	139
	4.6.4 CV measurement using Potassium Ferrocyanide.....	140
	4.6.5 DOE Results for GO Concentrations .....	141
	4.6.5(a) CV measurement for modified EC Sensor .....	143
4.7	Voltammetric Analysis of Pb <sup>2+</sup> and Cd <sup>2+</sup> on EC Sensor .....	144
4.8	Optimisation Study of the EC Sensor .....	146
	4.8.1 Accumulation Time.....	146
	4.8.2 Reduction Potential .....	147
	4.8.3 Reduction Time .....	148
	4.8.4 pH HCl Buffer Solution .....	148
4.9	Calibration and Limit of Detection Study of the EC Sensor.....	149
4.10	Summary .....	152
	<b>CHAPTER 5 CONCLUSION AND FUTURE RECOMMENDATIONS....</b>	<b>154</b>
5.1	Conclusion.....	154
5.2	Recommendations for Future Research .....	155
	<b>REFERENCES.....</b>	<b>157</b>
	<b>LIST OF PUBLICATIONS</b>	

## LIST OF TABLES

	<b>Page</b>
Table 1.1	Heavy metal sources in West Coast Peninsular Malaysia, according to the Malaysia Environmental Quality Report 2020.....3
Table 2.1	List of heavy metal sources, effects and standards. ....9
Table 2.2	Types of Material determine by ASV and CSV (March, Nguyen et al. 2015).....30
Table 2.3	Types of Heavy Metal detection technique and LOD.....31
Table 2.4	Classification various substrate properties. ....43
Table 3.1	Parameters for Randles-Sevcik equation ..... 78
Table 3.2	Sensor electrode's diameter specifications. ....79
Table 3.3	Cross-sectional area of sensor's electrode. ....80
Table 3.4	Electrode's resistance.....80
Table 3.5	EC Sensor design specification .....81
Table 3.6	Parameters for Faraday's Law of Electrolysis calculation .....85
Table 3.7	Parameters for electrochemical equivalent of gold.....86
Table 3.8	The electroplating sequence and associated parameters. ....89
Table 3.9	DOE for Generation 1 EC sensor..... 101
Table 3.10	DOE for Generation 2 EC sensor..... 101
Table 3.11	DOE for Generation 3 EC sensor..... 102
Table 3.12	DOE for GO Concentrations..... 103
Table 3.13	DPSV Parameters optimization..... 104
Table 3.14	DPSV measurement for Pb <sup>2+</sup> and Cd <sup>2+</sup> in real water. .... 104
Table 4.1	Parameters for GO dilution calculation..... 110
Table 4.2	Dilution summary for GO ..... 110

Table 4.3	Atomic percentage obtained from EDX results and the ratio of AgCl before and after measurement .....	124
Table 4.4	CV scans for peak current ratio for generation 1 EC Sensor. ....	127
Table 4.5	Summary of generation 1 EC sensor peak current ratio .....	127
Table 4.6	One-way Anova analysis for generation 1 EC Sensor.....	127
Table 4.7	CV scans for peak current ratio for generation 2 EC Sensor. ....	130
Table 4.8	Summary of generation 2 EC sensor peak current ratio .....	131
Table 4.9	One-way Anova analysis for generation 2 EC Sensor.....	131
Table 4.10	Peak current ratio for scan rate of 50 mV/s for RE in Au and Ag. ..	137
Table 4.11	Summary of generation 3 EC sensor peak current ratio .....	138
Table 4.12	One-way Anova analysis for generation 3 EC Sensor.....	138
Table 4.13	Anodic peak current, cathodic peak current and peak current ratio for different values of CV scan rates.....	139
Table 4.14	Anodic peak current, cathodic peak current and peak current ratio for different values of CV scan rates using Ferrocyanide for bare Au electrode. ....	140
Table 4.15	CV scans for peak current ratio for different concentration of GO. ....	141
Table 4.16	Summary of different concentration of GO peak current ratio .....	142
Table 4.17	One-way Anova analysis different concentration of GO.....	142
Table 4.18	Anodic peak current, cathodic peak current and peak current ratio for different values of CV scan rates using Ferrocyanide for modified GO/Au electrode.....	144
Table 4.19	Pb <sup>2+</sup> LOD standards. ....	150

## LIST OF FIGURES

	<b>Page</b>
Figure 2.1	Colourmetric sensing for heavy metal detection (Sener, Uzun et al. 2014). ..... 13
Figure 2.2	Paper-based colourmetric sensing for heavy metal detection (George and Senthilnathan 2017)..... 13
Figure 2.3	Magnetic relaxation switching for heavy metal detection (Liu, Cai et al. 2020)..... 14
Figure 2.4	Optical fiber for heavy metal sensing (Zhang, Sun et al. 2020). ..... 15
Figure 2.5	Electrochemical sensor block diagram (Cui, Wu et al. 2015)..... 16
Figure 2.6	Three electrode electrochemical sensing setup (Jin and Maduraiveeran 2018). ..... 16
Figure 2.7	Types of electrochemical setup (a) two electrode setup and (b) three electrode setup (Bard and Faulkner 2001). ..... 17
Figure 2.8	Classification for various electrochemical methods for heavy metal detection (Bansod, Kumar et al. 2017)..... 19
Figure 2.9	Potentiostat measurement setup (Martínez Gila, Estévez et al. 2022). ..... 20
Figure 2.10	Potential vs time (Banks, Foster et al. 2016). ..... 22
Figure 2.11	Potential changes (a) different scan rate applied and (b) graph view potential against time (Rajendrachari 2018). ..... 22
Figure 2.12	Potential wave with time changes (a); current response time (b) and (c) current vs potential (Gosser 1993)..... 24
Figure 2.13	Cyclic voltammetry (a) Excitation signal of cyclic voltammetry and (b) Cyclic voltammetry graph (Kissinger and Heineman 1983). ..... 25
Figure 2.14	Potential waveform for stripping voltammetry (Research 2020)..... 27

Figure 2.15	Effect of deposition potential on stripping voltammetry (Peterson and Wong 1981).....	28
Figure 2.16	Difference between ASV and CSV (Crapnell and Banks 2022).....	29
Figure 2.17	Types of commercial screen printed electrode (SPE) (Anshori 2023). ....	34
Figure 2.18	Types of substrates available for heavy metal sensor detection. ....	37
Figure 2.19	Electrolytic cell for electroplating (Paunovic and Schlesinger 2006). ....	44
Figure 2.20	Inert and active electrodes electroplating (a) carbon electrode at both polarity and (b) copper electrode as anode; carbon electrode as cathode (Baier and Witt 2014).....	46
Figure 2.21	Electrochemical sensor modification using drop-casting technique. ....	47
Figure 2.22	Crystal structures of different allotropes of carbon: graphene (2D); fullerene (buckyballs) (0D); nanotubes (1D) and graphite (3D) (Geim and Novoselov 2007). ....	49
Figure 2.23	Preparation of graphene oxide from graphite (Garg, Bisht et al. 2014). ....	52
Figure 2.24	Graphene Oxide synthesis methods comparison between HGO, IGO, and HGO+ (Marcano, Kosynkin et al. 2010).....	53
Figure 2.25	Simplified potentiostat diagram (Shen, Ju et al. 2020). ....	56
Figure 2.26	FESEM and EDX system.....	57
Figure 2.27	Matter-electron interactions, generation of (a) BSE, (b) SE, (c), x-rays (Kim and Park 2001). ....	58
Figure 2.28	Simplified schematics of FESEM-EDX system (Biswas and Gurao 2022). ....	60
Figure 2.29	Simplified schematics of TEM (Thomas and Gemming 2014). ....	61
Figure 2.30	HR-XRD system. ....	62
Figure 2.31	Illustration of Bragg's Law (Sochi 2010) .....	63

Figure 2.32	Operations of HR-XRD at $2\theta$ phase analysis (Husnain and Madhuku 2017). .....	64
Figure 2.33	(a) UV-Vis-NIR and (b) Simplified diagram of UV-Vis-NIR (Robles Fernández 2022). .....	66
Figure 2.34	(a) Simplified diagram of FTIR and (b) FTIR Spectrometer (Kumar 2018). .....	67
Figure 2.35	Simplified diagram of Raman spectroscopy (Smith and Dent 2019). .....	69
Figure 3.1	Methodology framework of this research work. ....	72
Figure 3.2	(a) Experimental setup for heavy metal sensor and (b) sensing mechanism of heavy metal sensor. ....	74
Figure 3.3	Generation 1 EC sensor CAD design.....	75
Figure 3.4	Generation 2 EC sensor CAD design.....	76
Figure 3.5	Heavy metal sensor (a) Overall dimension of the sensor (b) sensor's electrode dimension and (c) ratio between counter electrode with working electrode. ....	77
Figure 3.6	Heavy metal sensor overall fabrication process.....	83
Figure 3.7	Heavy metal ion sensor's electrode electroplating setup (a) photographed view of electroplating setup and (b) electroplating configuration. ....	89
Figure 3.8	Electroplating process (a) nickel plating (b) gold plating and (c) silver plating on reference electrode. ....	90
Figure 3.9	Overall summary of Graphene Oxide synthesis.....	92
Figure 3.10	Drop casting GO on EC sensor. ....	93
Figure 3.11	Microfluidic design and setup.....	94
Figure 3.12	Microfluidic casting process. ....	96
Figure 3.13	(a) Vacuum Chamber and (b) Sylgard® 184 from Dow Coning.....	97
Figure 3.14	(a) Wanhao duplicater 5S 3D printer and (b) Casting process for microfluidic. ....	97

Figure 3.15	Final fabricated heavy metal ion EC sensor integrated to microfluidic device.....	98
Figure 3.16	(a) Lab on PCB heavy metal detection setup and (b) graphical illustration for lab on PCB heavy metal detection setup.....	99
Figure 4.1	FESEM image of graphite flakes. The area circled in red has been magnified on the side to reveal more surface details. ....	107
Figure 4.2	FESEM image of graphene oxide. The area circled in red has been magnified on the side to reveal more surface details. ....	108
Figure 4.3	(a) TEM image of graphene oxide and (b) Magnified view to reveal more surface details.....	109
Figure 4.4	Series of different concentration of GO .....	109
Figure 4.5	FESEM image of all the diluted GO from 0.1 – 1.0 mg/ml.....	111
Figure 4.6	(a) Histogram about size distribution of GO flake size with fitted Gaussian profile and (b) the summary flake size distribution of various GO concentration. ....	113
Figure 4.7	Ultraviolet–visible absorption spectrum of GO. ....	114
Figure 4.8	Raman Spectrum of GO. ....	115
Figure 4.9	FTIR spectrum of GO and GO-SH .....	116
Figure 4.10	Model of GO functionalized with thiourea. ....	117
Figure 4.11	Copper Surface (a) before and (b) after treatment. ....	118
Figure 4.12	(a) FESEM image of electroplated nickel on copper surface and (b) Magnified view to reveal more surface details.....	118
Figure 4.13	FESEM imaging for Au surface on EC sensor - the area circled in red indicates a zoomed in view of the Figure. ....	119
Figure 4.14	XRD pattern of Au and Ni electroplated on Cu.....	120
Figure 4.15	FESEM imaging for silver surface on EC sensor - the area circled in red indicates an enlarged view of the Figure. ....	121
Figure 4.16	(a) Cross-section view for EC sensor and (b) estimate thickness of electroplated Ni, Au and Ag can be made using EDX line scan.....	122

Figure 4.17	FESEM imaging for AgCl before heavy metal detection. ....	123
Figure 4.18	FESEM imaging for AgCl after heavy metal detection. ....	124
Figure 4.19	Gen 1 EC sensor setup. ....	125
Figure 4.20	Cyclic voltammograms for first gen EC sensor. ....	126
Figure 4.21	(a) bubbles formation due to overpotential and (b) uncovered region of the EC sensor electrode. ....	128
Figure 4.22	Overpotential results (a) gold layer peeled off and (b) bubbles classification during overpotential. ....	129
Figure 4.23	FESEM Imaging for FR-4 surface morphology. ....	132
Figure 4.24	CV measurement for Tap water and ultrapure water. ....	134
Figure 4.25	Counter electrode characterisation with twelve different geometry. ....	135
Figure 4.26	CV measurement three times measurement from same EC sensor (a) Au as RE and (b) Ag/AgCl as RE. ....	136
Figure 4.27	CV measurement different geometry of CE (a) Au as RE and (b) Ag/AgCl as RE. ....	137
Figure 4.28	CV measurement using PBS buffer solution ....	139
Figure 4.29	Redox process for $K_4Fe(CN)_6$ .....	140
Figure 4.30	CV measurement for bare Au electrode.....	141
Figure 4.31	CV measurement for modified GO/Au electrode. ....	144
Figure 4.32	(a) Differential pulse stripping voltammetry of the modified GO/Au electrode and bare Au electrode in 40 $\mu\text{g/L}$ $\text{Pb}^{2+}$ . Experimental parameters: accumulation time of 15 minutes; reduction potential of -0.4 V; reduction time of 7 minutes; 0.1 M HCl buffer solution pH 4.0 and (b) Replication test results.....	145
Figure 4.33	(a) Differential pulse stripping voltammetry of the modified GO/Au electrode and bare Au electrode in (a) 40 $\mu\text{g/L}$ $\text{Cd}^{2+}$ . Experimental parameters: accumulation time of 15 minutes;	

	reduction potential of -0.4 V; reduction time of 7 minutes; 0.1 M HCl buffer solution pH 4.0 and (b) Replication test results.....	146
Figure 4.34	(a) Accumulation time on the stripping peak currents of the modified GO/Au electrode in 40 µg/L Pb <sup>2+</sup> and Cd <sup>2+</sup> . Experimental parameters: reduction potential -0.4 V; reduction time 7 minutes; 0.1 M HCl buffer solution pH 4.0 and (b) Replication test results. .	147
Figure 4.35	(a) Reduction potential on the stripping peak currents of the modified GO/Au electrode in 40 µg/L Pb <sup>2+</sup> and Cd <sup>2+</sup> . Experimental parameters: accumulation time 15 minutes; reduction time 7 minutes; 0.1 M HCl buffer solution pH 4.0 and (b) Replication test results. ....	147
Figure 4.36	(a) Reduction time on the stripping peak currents of the modified GO/Au electrode in 40 µg/L Pb <sup>2+</sup> and Cd <sup>2+</sup> . Experimental parameters: accumulation time 15 minutes; reduction potential -0.4 V; 0.1 M HCl buffer solution pH 4.0 and (b) Replication test results. ....	148
Figure 4.37	(a) pH effect of HCl buffer solution on the stripping peak currents of the modified GO/Au electrode in 40 µg/L Pb <sup>2+</sup> and Cd <sup>2+</sup> . Experimental parameters: accumulation time 15 minutes; reduction potential -0.4 V; reduction time 7 minutes. and (b) Replication test results. ....	149
Figure 4.38	Distribution of DPSV measurement of Cd <sup>2+</sup> and Pb <sup>2+</sup> .....	150
Figure 4.39	Differential pulse stripping voltammetry of the modified GO/Au electrode (a) Pb <sup>2+</sup> in the concentration of 10, 20, 40, 60, 80, 100 and 120 µg/L. Experimental conditions: accumulation time 15 minutes; reduction potential -0.4 V; reduction time 7 minutes; 0.1 M HCl buffer solution pH 4.0 (b) The standard curve for the modified GO/Au electrode.....	151
Figure 4.40	Differential pulse stripping voltammetry of the modified GO/Au electrode (a) Cd <sup>2+</sup> in the concentration of 10, 20, 40, 60, 80, 100 and 120 µg/L. Experimental conditions: accumulation time 15 minutes; reduction potential -0.4 V; reduction time 7 minutes; 0.1	

	M HCl buffer solution pH 4.0 (b) The standard curve for the modified GO/Au electrode.....	152
Figure 5.1	Proposed two-layer EC sensor with integration of heating element, op-amp chip and MCU.....	156

## LIST OF SYMBOLS

%	Percent
:	Ratio
~	approximately
≥	Greater than or equal to
2θ	Diffraction angle from XRD (measured in degree)
A	area
Å	Angstrom
C	carbon
°C	degree Celsius
D	Diffusion coefficient
E	Voltage
E <sub>c</sub>	Conditioning potential
E <sub>d</sub>	Deposition potential
E°	Standard electrode potential
g	gram
GPa	gigapascal
I	Current
I <sub>D</sub>	Intensity of D band in Raman
I <sub>G</sub>	Intensity of G band in Raman
I <sub>p</sub>	Peak current
I <sub>pa</sub>	Anodic peak
I <sub>pc</sub>	Cathodic peak
ℓ	liter
M	Molar mass
m	Meter

$t$	Time
$T_c$	Conditioning time
$T_d$	Deposition time
$T_e$	Equilibration time
$v$	Scan rate
$\Delta$	Changes
$\lambda$	x-rays wavelength
$\Omega$	resistor
%	Percent

## LIST OF ABBREVIATIONS

0D	Zero-dimensional
1D	One-dimensional
2D	Two-dimensional
3D	Three-dimensional
AAS	Atomic absorption spectrometry
ACS	American Chemical Society
Ag	Silver
Ag/AgCl	Silver/Silver Chloride
ASD	Autism spectrum disorder
ASV	Anodic stripping voltammetry
ATR	Attenuated total reflectance
Au	Gold
AUNPS	Gold nanoparticle
BSE	Backscattered electrons
CAD	Computer-aided design
Cd	Cadmium
CDC	Centre for Disease Control
CE	Counter electrode
CIS	CMOS image sensor
CMOS	Complementary Metal Oxide Semiconductor
Cr	Chromium
CSV	Cathodic stripping voltammetry
Cu	Copper
CV	Cyclic voltammetry
DI	Deionised
DP	Differential pulse
DPSV	Differential pulse stripping voltammetry
EC	Electrochemical
EDX	Energy dispersive x-rays
EEA	European Environment Agency
EQS	Environmental quality standards

Fe	Iron
FESEM	Field emission scanning electron microscopy
FR-4	Flame Retardant 4
FTIR	Fourier-transform infrared spectroscopy
GO	Graphene Oxide
Hg	Mercury
HRXRD	High-resolution X-ray diffraction
ICP-AES	Inductively coupled plasma atomic emission spectroscopy
ICP-MS	Inductively coupled plasma mass spectrometry
IPA	Isopropanol
LOC	Lab on Chip
LOD	Limit of Detection
LSV	Linear sweep voltammetry
LTCC	Low Temperature Co-Fired Ceramic
MEMS	Micro-electromechanical systems
Mg	Magnesium
NAA	Neutron activation analysis
Ni	Nickel
OSHA	Occupational Safety and Health Administration
PCB	Printed circuit board
PDMS	Polydimethylsiloxane
PET	Polyethylene Terephthalate
pH	Potential of Hydrogen
PV	Pulse voltammetry
RE	Reference electrode
SCE	Saturated calomel electrode
SE	Secondary electron
SPR	Surface plasmon resonance
SW	Square Wave
TEM	Transmission electron microscopy
USB	Universal Serial Bus
USEPA	US Environmental Protection Agency
UV	Ultraviolet
WE	Working electrode

WHO	World Health Organization
Zn	Zinc
μTAS	Micro Total Analysis Systems

# **PEMBANGUNAN PENDERIA LOGAM BERAT BERASASKAN MAKMAL DALAM PAPAN LITAR BERCETAK**

## **ABSTRAK**

Pencemaran logam berat di sumber air adalah masalah alam sekitar yang besar yang menimbulkan ancaman kepada kesihatan orang awam. Pengesanan elektrokimia adalah pendekatan yang menjanjikan untuk mengenal pasti dan mengkuantifikasi logam berat di dalam air kerana sensitiviti dan kebolehpilihannya yang tinggi. Walau bagaimanapun, elektrod kerja tradisional seperti karbon gelas dan merkuri tidak sesuai untuk penderia logam berat kerana kelemahan seperti sensitiviti rendah dan keracunan. Untuk menangani kelemahan ini, kajian ini bertujuan untuk meningkatkan reka bentuk dan kepelbagaian fabrikasi penderia elektroanalisis dengan mengimplementasikan teknik fabrikasi Papan Litar Bercetak (PCB) konvensional. Sensor yang difabrikasi telah mencapai pengecilan saiz sebanyak 40% berbanding dengan sensor elektrokimia sedia ada. Menurut pengukuran voltammetri berkitar (CV), penderia yang difabrikasi dapat menghasilkan tindak balas puncak yang berulang dengan kadar pengimbasan yang berbeza antara 100 mV/s hingga 10 mV/s dengan mencapai nisbah arus puncak sebanyak 1. Graphene Oxida (GO) yang telah diubah suai sebanyak 0.2 mg/ml pada elektrod kerja telah diterokai sebagai bahan penderia kerana sensitiviti dan kebolehpilihannya yang tinggi dalam mengesan logam berat seperti plumbum dan kadmium, dengan peningkatan sebanyak 45% dalam pengesanan logam berat ini. Keadaan optimum untuk pengesanan plumbum dan kadmium ditentukan dengan masa pengumpulan selama 10 minit, potensi penurunan -0.4 v, masa penurunan selama 7 minit, dan pH 4.0 penyelesaian penampakan HCL 0.1 M. Keputusan menunjukkan elektrod kerja GO menunjukkan peningkatan sensitiviti dan kebolehpilihan

berbanding dengan elektrod tradisional dengan julat linear 10  $\mu\text{g/L}$  hingga 120  $\mu\text{g/L}$  kepekatan, dan *Limit of Detection* (LOD) sebanyak 32 ppb dan 28 ppb untuk plumbum dan kadmium, masing-masing. Nilai-nilai ini berada dalam piawaian WHO yang dibenarkan, yang memerlukan LOD sebanyak 50 ppb untuk Pb dan 10 ppb untuk Cd.

# **DEVELOPMENT OF LAB ON PRINTED CIRCUIT BOARD BASED HEAVY METAL DETECTION**

## **ABSTRACT**

Heavy metal contamination in water sources is a significant environmental problem that poses a threat to public health. Electrochemical detection is a promising approach to detecting and quantifying heavy metals in water, due to the high sensitivity and selectivity it provides. However, traditional working electrodes, such as glassy carbon and mercury, are not ideal for detecting heavy metals due to limitations such as low sensitivity and toxicity. To address these limitations, this study aimed to improve the design and fabrication complexity of electro-analytical sensors by implementing a conventional Printed Circuit Board (PCB) fabrication technique. The fabricated sensor has achieved miniaturization of 40% compared to existing electrochemical sensors. According to cyclic voltammetry (CV) measurements, the fabricated sensor can produce a reversible peak reaction with different scan rates between 100 mV/s to 10 mV/s achieving a peak current ratio of 1. The modified Graphene Oxide (GO) of 0.2 mg/ml on the working electrode was explored as a sensing material due to its high sensitivity and selectivity in detecting heavy metals such as lead and cadmium, with an improvement of 45% in the detection of these metals. The optimum conditions for the detection of lead and cadmium were determined with a 10-minute accumulation time, -0.4 v reduction potential, 7-minute reduction time, and pH 4.0 of 0.1 M HCL buffer solution. The results showed that the GO working electrode demonstrated improved sensitivity and selectivity compared to traditional electrodes, with a linear range of 10 µg/L to 120 µg/L concentration, and a LOD of 32 ppb and 28 ppb for lead and cadmium, respectively. These values were

within the permitted WHO standards, which require a LOD of 50 ppb for Pb and 10 ppb for Cd.

# CHAPTER 1

## INTRODUCTION

### 1.1 Overview

The term "heavy metal" refers to a group of metals and metalloids with atomic densities more than  $5 \text{ g/cm}^3$  (Aprile and De Bellis 2020). Heavy metal is also defined as having a molecular weight of more than 40 (Duffus 2001). A light metal is any metal having a molecular weight of less than 40. Heavy metals are naturally occurring substances in the Earth's crust. They get into our bodies in minute amounts from food, water, and air. They cannot be destroyed or degraded in any way (Mishra, Bharagava et al. 2019). Copper is one of the metals that man has been using since the dawn of time. Copper was the first metal found by man back in 9000 BCE. Gold, silver, tin, lead, and iron was among the other metals used in prehistoric times. Since the discovery of the copper metal, humanity has begun the copper age, the bronze age and the iron age (Rehman, Liu et al. 2019). These ages show that humanity heavily relies on metal to craft our modern society today. However, everything comes with a price to pay. Heavy metal contamination has become a global concern due to the rapid development of industry and manufacturing. Heavy metals like Cd, Pb, and Hg have gotten much press because of their high toxicity, which affects our daily health. Heavy metals are also non-biodegradable elements, posing a risk to human health (Ahmad, Alharthy et al. 2021). Mercury was identified in banned skin-lightening cosmetics and fluorescent bulbs, for example (Ricketts, Knight et al. 2020). Meanwhile, chromium is obtained through mining and leather tanning, cadmium is obtained through zinc smelting and paint sludge, and lead is obtained through lead-acid batteries and coal-fired power plants (Xiong, Liu et al. 2019).

## 1.2 Heavy Metal Pollutions in Malaysia

Malaysia is a recent industrial growth country with an industrial economy experiencing rapid growth (Salam, Paul et al. 2019). The increased production and harmful compounds such as trace elements have come from rapid expansion and economic growth through land development, urbanisation, and industrialisation (Siwar, Ghazali et al. 2022). Heavy metal pollution also causes river pollution, agricultural soil toxicity, and other problems. Sungai Perai, Sungai Perak, and Sungai Linggi, in particular, were long thought to be heavily polluted by pollutants, toxic metals, and sewerage. The surficial sediment of heavy metal from Sungai Perai was found with Pb, Cd, Cu, Cr and Zn were  $28.6 \pm 6.84$ ,  $0.42 \pm 0.32$ ,  $21.8 \pm 9.05$ ,  $66.0 \pm 28.1$  and  $74.7 \pm 33.3$   $\mu\text{g/g}$  dry weights, respectively (Foo, Ecklyn et al. 2021). Moreover, in Sungai Perak, trace of heavy metal also discover as such: Fe, Cu, Cd, Zn and Pb were  $20.24 \pm 56.58$ ,  $6.6 \pm 19.12$ ,  $1.51 \pm 3$ ,  $20 \pm 51.27$  and  $14.56 \pm 27$   $\mu\text{g/g}$  dry weights (Salam, Paul et al. 2019). Furthermore, the occurrence and distribution of heavy metal in Sungai Linggi are Pb, Ni, Mg, Fe, Cu and Cd were 0.10, 0.24, 14.41, 45.77, 0.37 and 0.49 ppb (Razak, Aris et al. 2021).

Aside from water contamination, surface sediments have become the primary reservoir for the heavy metal pollutant. Table 1.1 depicts the sources of heavy metals input on Peninsular Malaysia's west coast, covering manufacturing industries, agricultural and aquaculture, agro-based businesses, and urbanisation activities (Sany, Tajfard et al. 2019). According to the Malaysia Environmental Quality Report 2020, the primary sources of water pollution are manufacturing industries (2.17 %), sewage treatment plants (34.46 %), pig farming (33.74 %), agro-based industries (29.14 %), and wet markets (0.49 %), with Johor state having the most water pollution sources,

followed by Perak and Selangor. The primary types of scheduled waste created in the nation were dross/ slag/ clinker/ ash, heavy metal sludge, and gypsum. (Sekitar 2020).

The primary industries that contribute to the rising quantity of scheduled waste created annually include power plants, water treatment facilities, chemical industries, metal refineries, and electric and electronic industries (Chin and Yong 2019). The regulatory standards for discharges from human activities and companies containing process plants should be strictly enforced. Not just for environmental and health reasons, but also as a resource conservation measure, wastes containing heavy metals should be reprocessed or recycled more frequently.

Table 1.1 Heavy metal sources in West Coast Peninsular Malaysia, according to the Malaysia Environmental Quality Report 2020.

<b>Sources</b>	<b>Type of Industry/ Products</b>
Manufacturing Industries	Battery Electroplating Fertilizers Gasoline Leather Ore Processing Paint Pesticides Pipe Plastic Printing Silver Refineries Smelting Steel Textile Toy-making Wall Paper
Agriculture and Aquaculture	Agrochemicals Inorganic fertilizers
Agro based Industries	Rubber

	Palm oil
	Paddy
Urbanization	Domestic discharge
	Leachate
	Sewage sludge

---

### 1.3 Problem Statement

Electrochemical sensors have significant potential for various applications, including environmental monitoring, medical diagnosis, and industrial quality control. However, one of the major challenges in their widespread adoption is the design and fabrication complexity of the electrodes used in these sensors. The current electrode fabrication methods often involve multiple steps and can be time-consuming and costly, making it difficult to produce the sensors in large quantities. Conventional Printed Circuit Board (PCB) fabrication techniques offer a potential solution to this problem, as they allow for the creation of complex patterns with high precision and reproducibility. However, there is a need for further research to develop an improved electrode design and fabrication process that is compatible with PCB technology. (Scott and Ali, 2021; Solhi et al., 2020)

The contamination of the environment with heavy metals is a significant environmental problem that poses numerous health risks. Electrochemical detection is a promising approach for detecting and quantifying heavy metals due to its high sensitivity and selectivity. However, traditional working electrodes such as glassy carbon and mercury are not ideal for heavy metal detection due to limitations such as low sensitivity and toxicity. As a result, alternative sensing materials such as bismuth, gold nanoparticles, and carbon-based materials have been explored to overcome these limitations. Nevertheless, the modification of working electrodes is still necessary to enhance their performance. In this regard, the gold (Au) working electrode has shown

promise in detecting heavy metals such as lead and cadmium. (Hu et al., 2020; Wang et al., 2018)

The detection of pollutants in water is a critical environmental concern, and the World Health Organization (WHO) has established guidelines and standards for various pollutants in drinking water. Electrochemical sensors have shown significant potential for the detection of pollutants in water due to their high sensitivity and selectivity. However, in order to determine the suitability of these sensors for practical applications, it is necessary to evaluate their limit of detection (LOD) using real water samples. The LOD is the lowest concentration of a pollutant that can be detected by the sensor, and it is an important parameter for assessing the performance of the sensor. (Scott and Ali, 2021; Solhi et al., 2020; WHO, 2017)

#### **1.4 Research Objective**

This research aims to design and fabricate a heavy metal sensor platform using the available printed circuit board technology. Advanced PCB technology research will give rise in next-generation PCB technology from a system onboard (SoB). In order to obtain a higher sensing performance, additional sensing material was synthesis to study the compatibility of the heavy metal sensor. Hence, this research was carried out to accomplish three main objectives:

- i. To improve the electrode's design and fabrication complexity through the implementation of conventional Printed Circuit Board fabrication technique.
- ii. To modify the Au working electrode with graphitic material and determine the optimum condition for lead and cadmium ions detection.

- iii. To perform the evaluations of the limit of detection for the fabricated PCB sensor with real water samples within WHO standards

## **1.5 Research Scope and Limitation**

This research is embark based on the following scope:

This research focuses on developing lab on PCB for heavy metal detection specifically  $Pb^{2+}$  and  $Cd^{2+}$  due to its severe hazard towards human health especially kidney damage and impaired growth in children (Lee, Idrus et al. 2021, Razak, Aris et al. 2021), which is later demonstrated in designing, fabricating, and characterising sensor performance. Towards to simplification and less complexity fabrication, this sensor was focus on utilising the conventional PCB technique to fabricate the sensor. The FR-4 substrates offer high thermal stability, mechanical and electrical qualities, and resistance to the majority of routinely used chemicals. (Pecht, Agarwal et al. 2017). PCB technology benefits from fabrication services, large-scale production, dependability, and electronic integration. Finally, recycling and disposal facilities for disposable lab-on-PCBs are now built and in use in the PCB sector, alleviating environmental concerns (Mir and Dhawan 2022).

## **1.6 Organization of Thesis**

Chapter 2, the literature review, focus on the concepts of heavy metal, the available heavy metal sensors, electrochemical sensing technique, electrochemical sensor design and fabrication, sensing graphene oxide synthesis, system integration in microfluidic and characterization instruments.

Chapter 3 focuses on discussing the entire process of design, fabrication and synthesis of the heavy metal sensor based on the fundamentals and theory available from literature review. The process elaborates the method, approaches, equipment, and precaution conducted throughout the flow of the present study. In addition, the design of experiment for the fabricated sensor, sensing material GO and optimization in heavy metal sensing.

Chapter 4 presents the experimental findings and discussion of this project. In this chapter, all related findings, measurement and DOE results were documented in this section as the sequence began from GO synthesis, sensor characterisation, sensor LOD optimization and real water testing.

Chapter 5 concludes the overall progress. In addition, the recommendation for further studies is also discussed based on the limitations observed in the present study.

## **CHAPTER 2**

### **LITERATURE REVIEW**

#### **2.1 Overview**

This chapter provides an overview of the heavy metal sensor. The discussion will distribute among the exposure of heavy metal, the available heavy metal sensor, electrochemical sensing techniques, sensor fabrication, synthesis of graphene oxide, application of electrochemical sensor in microfluidic system and related instrument for characterization.

#### **2.2 Heavy Metal Exposure**

Excessive heavy metal exposure poses a serious threat to human life. The primary sources of human exposure were soil, food, and water. The effect of heavy metal poison on children was the most severe due to age growth. Autism spectrum disorder (ASD) is a neurodevelopmental disorder characterised by symptoms that impair affected individuals' quality of life, such as social interaction deficit, cognitive impairment, intellectual disabilities, and restricted and repetitive behavioural patterns. Environmental metal poisoning has been linked to the pathogenesis of ASD. Congenital rubella is linked to early evidence of environmental influence on neurodevelopmental disorders associated with an increased rate of autism (Ijomone, Olung et al. 2020). During industrial processes, heavy metal elements such as lead (Pb) and cadmium (Cd) always cause environmental issues. Both of these metals are non-biodegradable and may accumulate in the ecological system over time, causing serious pollution to people's health. The heavy metals to be detected in this study were lead (Pb) and cadmium (Cd). Each of the heavy metal bands chosen has its own distinct characteristics.

Metals are necessary for cellular functions, but their concentration range significantly impacts human health. It is considered safe if the concentration range of metals is less than the toxicity range. However, if it exceeds the allowable limits, it will influence biochemical processes in a cell, causing cell mutagen and cancer. Table 2.1 shows heavy metal contaminations and their toxicity ranges according to WHO.

Table 2.1 List of heavy metal sources, effects and standards.

Heavy Metals	WHO limits (µg/L)	Sources	Effects	References
Mercury (Hg)	1	Corps preservation, human activities like as fossil fuel combustion, chlor-alkali industries, mining, and the usage of coal and petroleum	Neurological disorder, Uncontrolled limb movements, poor motor skills, impaired speech, poor vision, and hearing	(Paduraru, Iacob et al. 2022)
Chromium (Cr)	50	Metallurgy, papermaking, electroplating and Leather industry	Chronic poisoning, teratogenic, Carcinogenic, Mutagenic effect, and allergic to human	(He, Gu et al. 2020) (China, Maguta et al. 2020)
Cadmium (Cd)	5	Mining, smelting, coal combustion, Cd electroplating sector, the chemical plants, fertiliser manufacture, and waste incineration	Chronic obstructive pulmonary disease (COPD), Emphysema, Bronchitis, Chronic rhinitis, kidney and liver failure, Carcinogenic	(Wang, Chen et al. 2021)
Lead (Pb)	50	Battery plates, soldering compounds, guards in atomic reactors, and radioactive material containers, paint ceramics, and construction industries, bearing manufacture, printing, and aircraft gasoline	Cardiovascular effect, birth defects, respiratory effect, neurological effect, reproductive effect, cause mutations and congenital abnormalities in the fetus.	(Charkiewicz and Backstrand 2020)

Lead poisoning one of the most severe and pernicious effects of environmental pollution. While the use of lead in certain products, such as gasoline and paints, has been banned or significantly reduced on a global scale, lead poisoning continues to impose significant costs on society, notably in small- and middle-income countries, due to the ongoing use of lead in different products, mining and smelting activities, and a lack of mitigation for polluted areas (Shabani, Hadeiy et al. 2020). Lead ingestion at high levels has a detrimental effect on the circulatory and neural systems. It can be deadly in severe circumstances, although low-level exposure can impair cognitive ability and cause developmental abnormalities. Additionally, adverse health consequences might result in decreased academic performance, decreased educational attainment and lifetime earnings, and behavioural issues (Yamada, Hiwatari et al. 2020).

Cadmium (Cd) is a well-known hazardous element found in drinking water, air, and soil. Individuals can readily become exposed to Cd through regular activities such as smoking and consuming excessive Cd content foods. Numerous clinical data indicate that Cd is harmful to various organs and tissues, including the blood, bone, liver, kidney, lung, testis, and brain. Since it has a long biological half-life (15 to 20 years), Cd can attach to proteins in the blood, such as albumin and certain immunoglobulins, and then internalise and accumulate in neuronal cells via fluid-phase endocytosis. Cd can easily cross the blood-brain barrier and accumulate in the nervous system, resulting in central nervous system (CNS) dysfunction, including migraine and vertigo, olfaction dysfunction, peripheral neuropathy, vascular function slowing, balance disorder, cardiorespiratory, attention deficit hyperactivity disorder, and intellectual disabilities (Zhao, Yu et al. 2020).

The Centers for Disease Control and Prevention (CDC), European Environment Agency (EEA), Occupational Safety and Health Administration (OSHA), United States Environmental Protection Agency (USEPA), and World Health Organization (WHO) have identified heavy metals as priority constituents to be monitored and established permissible limits for their concentrations in water under environmental quality standards (EQS). (Gumpu, Sethuraman et al. 2015, Sneddon and Vincent 2008). As a result, sensitive and selective technologies for verifying the trace levels of these hazardous heavy metal ions in diverse complex matrices, such as biological samples (blood, serum, urine, saliva), natural and wastewater, food, soil, and air, have emerged.

### **2.3 Heavy Metal Sensor**

Heavy metals above a particular threshold limit are hazardous to people and can induce various life-threatening disorders, as we all know. Traditional heavy metal detection methods included atomic absorption spectrometry (AAS), spectrophotometry, and inductively coupled plasma mass spectrometry in the early years (ICP-MS). Because of its excellent sensitivity and selectivity, AAS is one of the most widely used metal and metalloid trace analysis techniques. The initial step in AAS is to atomise the sample analyte utilising flame atomisers, electrothermal atomisers, or vapour generation atomisers. The second stage is the absorption of electromagnetic radiation at a wavelength specific to analyte atoms. ICP-MS combines the inductively coupled plasma (ICP) and mass spectrometry (MS) techniques (MS). For quantitative analysis, the absorption signal recorded in atomic absorbance is connected to the concentration of free analyte atoms. The operational concept of ICPMS is the same as that of AAS, with sample analyte atomization in ICP and

radiation absorption by analyte atoms in MS. Both AAS and ICP-MS offer great precision, sensitivity, and selectivity for heavy metals determination. They do, however, have the drawback of high maintenance expenses, the need for skilled personnel, and the fact that they are primarily laboratory bound. As a result, delays in detecting and estimating these metal pollutants in drinking water samples have been linked to various human health problems. Therefore, it is critical to continue monitoring harmful metals levels in water supplies and maintain a steady supply of safe drinking water. As a result, a simple, sensitive, cost effective, and direct analysis method is required to detect heavy metal ions. Numerous strategies have been developed for monitoring heavy metals. Colourimetric (optical), magnetic relaxation, optical fiber sensor, and electrochemical sensors. The following subsections discuss the fundamental principles and applications of the approaches.

### **2.3.1 Colorimetric sensing**

The colourimetric array typically necessitates the direct or indirect interaction of heavy metal ions with nanomaterials or biomolecules such as aptamers and enzymes. Paper, hydrophobic membranes, 96-well plates, and other carriers are all compatible with the colourimetric array (Yu, Pang et al. 2021). In a nutshell, heavy metal's presence causes changes in the reflection properties of a solution, such as colour and wavelength. The type of heavy metal and its concentration in a solution determine the variations (Yan, Yuan et al. 2020). As shown in Figure 2.1, cadmium ions were dispensed into the gold nanoparticle solution. After the chemical reaction between cadmium and gold nanoparticles, the solution changes red to blue. The colourimetric sensors detect pollutants by a visual and visible colour change that can be seen with the naked eye, making them a very fast-responding detector (Saxena, Jain et al. 2021).

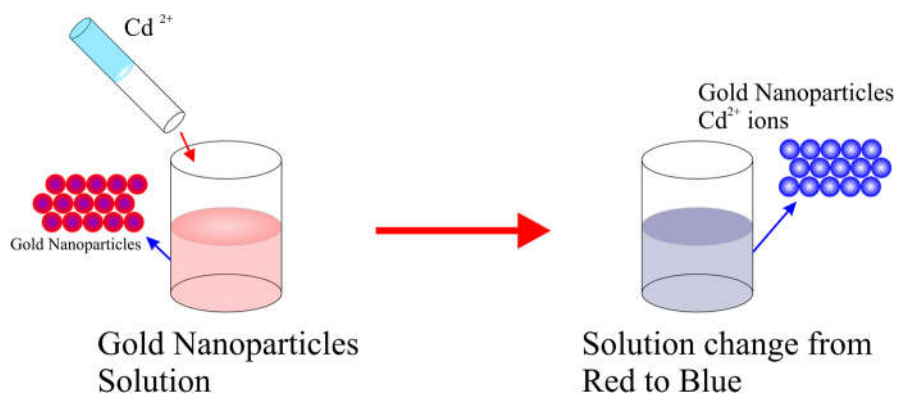


Figure 2.1 Colourimetric sensing for heavy metal detection (Sener, Uzun et al. 2014).

Another colourimetric sensor was created on a paper strip, and when the colourimetric paper strip was immersed in  $\text{Hg}^{2+}$  ion solution, a distinct colour change from yellow to grey/black was observed. The sensor had an excellent linearity range of 1–20 M and a limit of detection 82.66 nM. Figure 2.2 depicts the green synthesis of AgNPs and colourimetric detection of  $\text{Hg}^{2+}$  ions (George and Senthilnathan 2017).

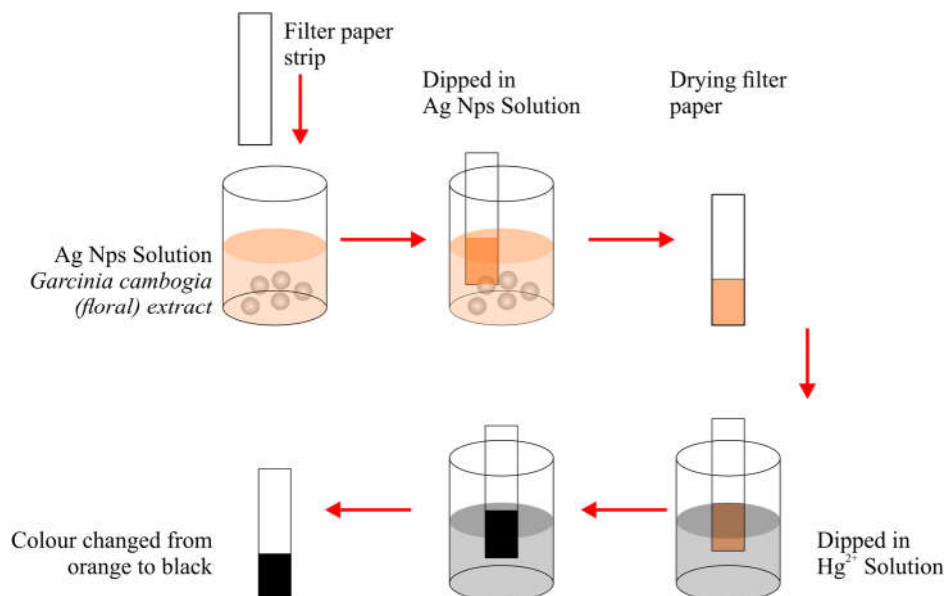


Figure 2.2 Paper-based colourimetric sensing for heavy metal detection (George and Senthilnathan 2017).

Numerous advancements have accomplished in the field of colourimetric sensors to detect heavy metals. However, this approach is insensitive and selective, kinetically unstable, and unsuitable for use in aquatic conditions.

### 2.3.2 Magnetic relaxation sensor

Magnetic materials are employed in this technology to create sensitive systems based on magnetism principles. Magnetic nanoparticles (5–100 nm in diameter) or magnetic particles (300–5,000 nm in diameter) are used to identify specific heavy metal targets. Depending on the sort of target intended, particles are often surface functionalized. As illustrated in Figure 2.3, an MRS based on  $\text{Fe}_3\text{O}_4$  nanoparticles (NPs) was made. In particular, the concentrations of  $\text{Hg}^{2+}$  in industrial pollutants are typically well above the detection limit. As a result, gold nanoparticles (AuNPs) were synthesised on the surface of  $\text{Fe}_3\text{O}_4$  nanoparticles to enable visual detection of  $\text{Au}@\text{Fe}_3\text{O}_4$  nanoparticles.  $\text{Hg}^{2+}$  in the sample can cause the agglomeration of  $\text{Au}@\text{Fe}_3\text{O}_4$ -aptamers NPs via T- $\text{Hg}^{2+}$ -T base pairs, resulting in displacement of the detection solution's transverse relaxation time  $T_2$  value (Liu, Cai et al. 2020).

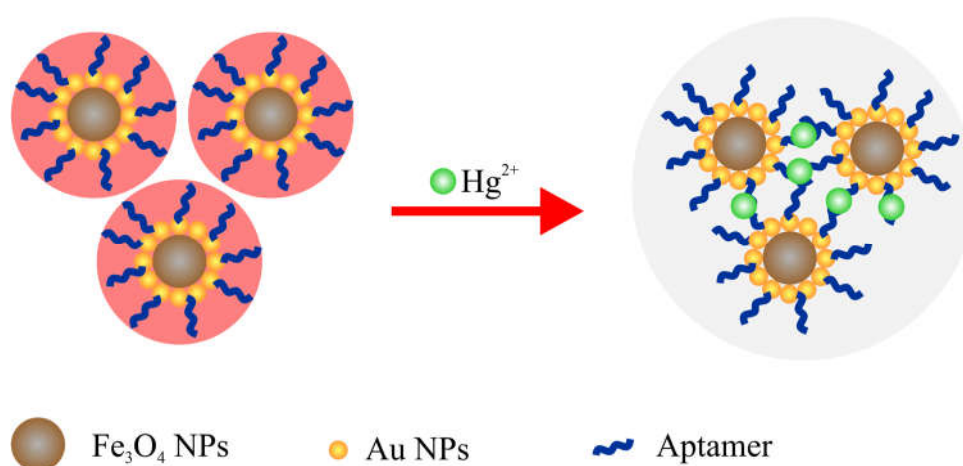


Figure 2.3 Magnetic relaxation switching for heavy metal detection (Liu, Cai et al. 2020).

### 2.3.3 Optical Fiber Sensor

The optical fibre in the heavy metal ion sensor uses sensitive material to detect heavy metal ion. As illustrated in Figure 2.4, the sensing region is initially illuminated by light projected from an optical source via an optical fibre. The sensing region of the optical fibre is coated with a material that is sensitive to heavy metal ions and changes its refractive index or volume in response to changes in heavy metal ion concentration. As a result, when the light signal interacts with the light reactive material, its wavelength, intensity, phase, or polarisation state changes in lockstep with the variation in the concentration of heavy metal ions. The light signal containing the sensing data is then transferred to a photodetector for demodulation. As a result, the sensitive region is the critical component of the sensing system, as it directly determines the sensing properties of the heavy metal ion sensor. Lastly, the measured concentration of heavy metal ions can be monitored by observing changes in the optical fibre output signal (Zhang, Sun et al. 2020).

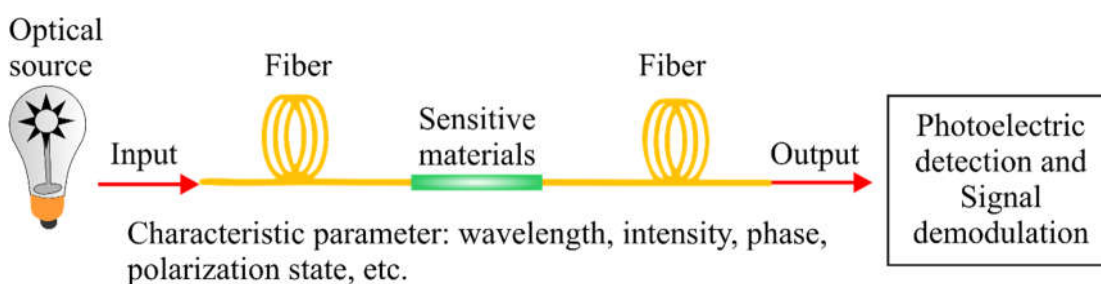


Figure 2.4 Optical fiber for heavy metal sensing (Zhang, Sun et al. 2020).

### 2.3.4 Electrochemical Sensor

Typically, an electrochemical cell comprised of an ionic conductor (an electrolyte) and an electronic conductor is used to detect heavy metal ions electrochemically (an electrode). For this case, the electrolyte is an aqueous solution containing heavy metal ions. An electrochemical experiment generally uses an

external power supply to generate an excitation signal and determine the response function in a chemical solution while holding numerous system variables constant. At the electrode-electrolyte solution interaction, the cell potential is measured. In the electrolytic cell, numerous half-reactions occur, one of which occurs at the working electrode (WE). The other electrode against which the cell potential is measured is known as the reference electrode (RE) as illustrated in Figure 2.5.

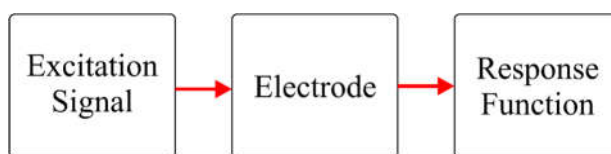


Figure 2.5 Electrochemical sensor block diagram (Cui, Wu et al. 2015).

The third electrode in a three-electrode cell layout is referred to as the counter electrode (CE). The current is typically passed between the WE and the CE. Figure 2.6 displays a general three-electrode cell configuration for electrochemical detection of heavy metal ions in an aqueous solution.

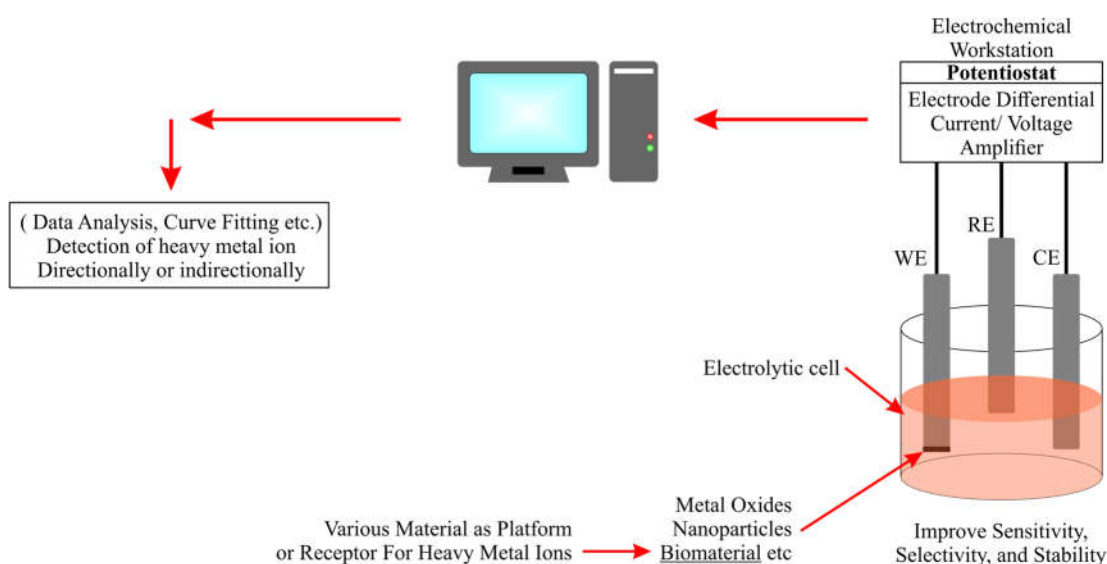


Figure 2.6 Three electrode electrochemical sensing setup (Jin and Maduraiveeran 2018).

As previously stated, three electrodes are used in an electrolytic cell with WE modified with different interface materials as a platform for heavy metal ions. The current is typically passed between the WE and CE in this electrochemical setup. Some glass separators are used to separate the CE from the WE, and the material is inlet so that it does not affect the WE. Prior to prevent current from being drawn from the RE, the potential is measured between the WE and RE using a high input impedance device. These electrodes are electrically connected to an electrochemical workstation, laboratory equipment, or portable in-field device with an inbuilt power source to provide excitation signals to the electrode setup and measurement units to receive and measure the response signals. The electrochemical workstation is linked to a computer that has been pre-loaded with the software platforms needed to interpret and analyse the experimental data. A two-electrode cell setup with WE and RE is used to measure the electrode potential for solutions with low solution resistance. Figure 2.7 depicts a two-electrode cell configuration (a). For electrochemical experiments involving nonaqueous solutions with low conductivities and higher solution resistances, a three-electrode cell setup with WE, RE, and CE is used, as shown in Figure 2.7(b).

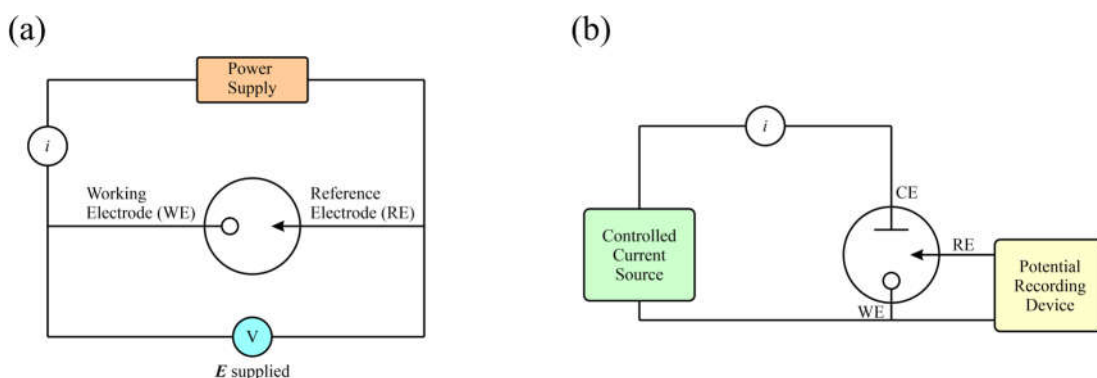


Figure 2.7 Types of electrochemical setup (a) two electrode setup and (b) three electrode setup (Bard and Faulkner 2001).

Potentiostatic and galvanostatic measurement techniques are widely used in the field of electrochemistry due to their ability to measure the two parameters of

current and potential, which cannot be controlled simultaneously. However, there are also methods where no control signal is necessary, such as when the current is optimal and the potential across the electrodes is zero. Potentiometric techniques are frequently used to identify heavy metal ions by measuring the potential, but there are also other techniques available, such as impedance measurement techniques, which measure changes in double-layer capacitance, solution resistance, and charge transfer resistance in response to the availability of heavy metal ions.

Furthermore, electrochemiluminescence is another approach that is extensively used to estimate the concentration of heavy metal ions in response to the luminescence effect generated during the experiment. These methods rely on various measurement signals to determine the type and concentration of heavy metal ions in the electrolyte and require the use of numerous electroanalytical instruments. Among these instruments, high input impedance potentiometers, potentiostats, galvanostats, and impedance measuring devices are the most commonly used. Moreover, it is essential to note that the accuracy and precision of these electroanalytical instruments depend on various factors such as the sensitivity of the electrodes, the quality of the electrolyte, and the stability of the instrument over time. Therefore, it is crucial to ensure proper calibration and maintenance of these instruments to obtain reliable and consistent results. Additionally, the development of advanced electroanalytical instruments with improved sensitivity and selectivity is continuously being pursued to enhance the accuracy and efficiency of heavy metal ion detection. Figure 2.8 illustrates a detailed classification of electrochemical sensing techniques for detecting heavy metal ions (Bansod, Kumar et al. 2017).

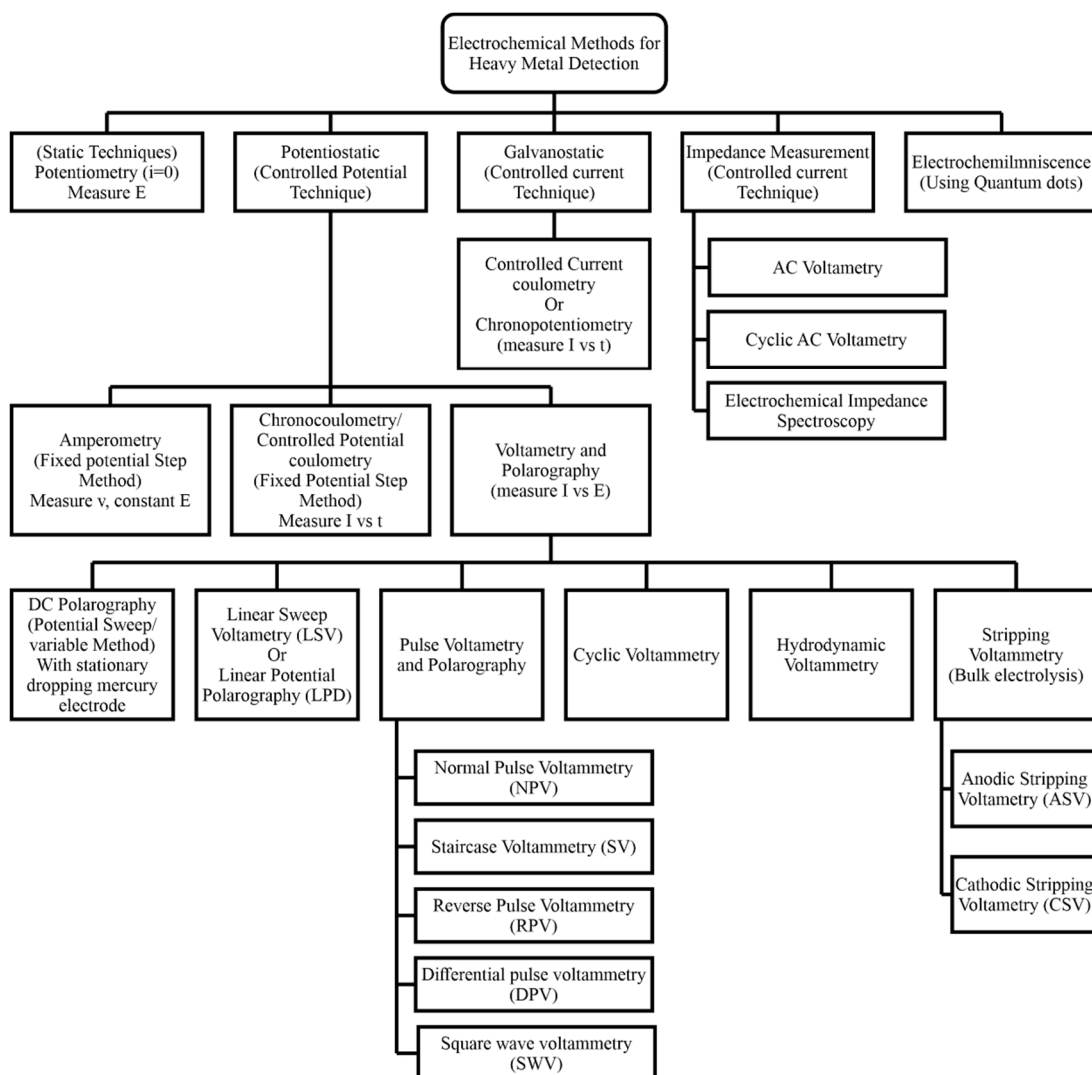


Figure 2.8 Classification for various electrochemical methods for heavy metal detection (Bansod, Kumar et al. 2017).

### 2.3.4(a) Potentiostatic technique

Potentiostatic techniques entail using a potentiostat instrument to control the potential between its RE and CE to maintain a stable potential difference between the RE and WE, as shown in Figure 2.9. The resulting current is measured and recorded to estimate the analytes' concentration. These types of experiments are also known as potential controlled techniques. These controlled potential techniques are further categorized according to the type of voltage signal used and the resulting measured current waveforms. The three major subcategories of potentiostatic techniques are amperometry, chronocoulometry, and voltammetry/polarography.

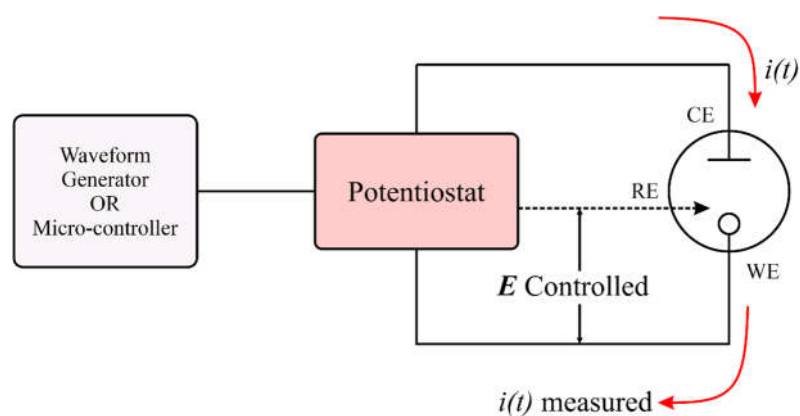


Figure 2.9 Potentiostat measurement setup (Martínez Gila, Estévez et al. 2022).

### 2.3.4(b) Amperometry

Amperometry is an electroanalytical technique that entails applying a steady reducing or oxidising potential to a working electrode and measuring the faradaic current (Amine and Mohammadi 2019). A potential step signal is provided between the reference and working electrodes in a solution containing the target electroactive analyte. The reduction reaction occurs at the electrode surface, resulting in a high current flow proportionate to the concentration change at the electrode surface. The resulting current is plotted against time. This approach is confined to identifying a single component from an electrochemically reducible species based on the working electrode's fixed potential.

### 2.3.4(c) Chronocoulometry

Chronocoulometric techniques are Amperometric techniques' integral analogues. These methods measure the amount of charge passed after applying a controlled potential calculated by taking the integral of current vs time or voltage. These methods are primarily used to perform exhaustive electrolysis for quantitative analysis, but they provide very little information about the analyte type. Chronocoulometric techniques are used to determine the extent of adsorption of species that undergo reaction at the electrode surface in electroactive materials. In

contrast to other amperometric and voltammetric techniques, this electrolysis is done at constant current rather than constant potential. Chronocoulometry, unlike amperometric techniques, employs larger surface area electrodes, resulting in higher efficiency due to the analyte's near-complete reaction. Although this technique offers high precision and simplicity, it necessitates a high current efficiency, so it is not widely used for electrochemical analysis.

#### **2.3.4(d) Voltammetric techniques**

In order to determine and measure heavy metal ions in a variety of complex environmental matrices, voltammetric techniques are often commonly used. Compared to the fixed potential point used in amperometric techniques, these techniques measure current at various potential points along a current-voltage curve. Because of its high accuracy and sensitivity, voltammetry is a widely used technique for identifying traces of heavy metal ions. These methods are well suited to suppressing the background current and increasing the detection limit. The reversibility of reactions in the electrochemical cell setup can be used to obtain qualitative information.

Linear sweep voltammetry (LSV), Pulse voltammetry (PV), cyclic voltammetry (CV), and stripping voltammetry (SV) can be further classified as anodic stripping voltammetry (ASV) or cathodic stripping voltammetry (CSV) depending on the type of current-voltage curve resulting from the analysis methods (CSV).

#### **2.3.1(d)(i) Linear sweep voltammetry**

Linear sweep voltammetry is a broad term for any voltammetric method in which the potential applied to the working electrode changes linearly over time. To measure the resulting I-E curve, the applied potential is typically between (10 mV/s

and 1000 mV/s). As shown in Figure 2.10, the slope of this ramp has units of volts per unit time and is commonly referred to as the scan rate.

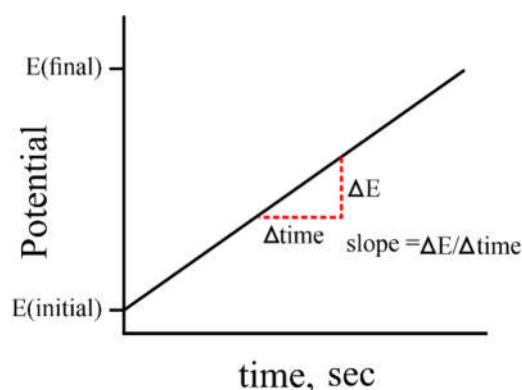


Figure 2.10 Potential vs time (Banks, Foster et al. 2016).

The line slope is used to determine the voltage scan rate (v). By alter the scan rate, the time require to sweep will be different. The rate of the electron transfer reaction, the chemical reactivity of the electroactive species, and the voltage scan rate all influence the characteristics of the recorded linear sweep voltammogram.

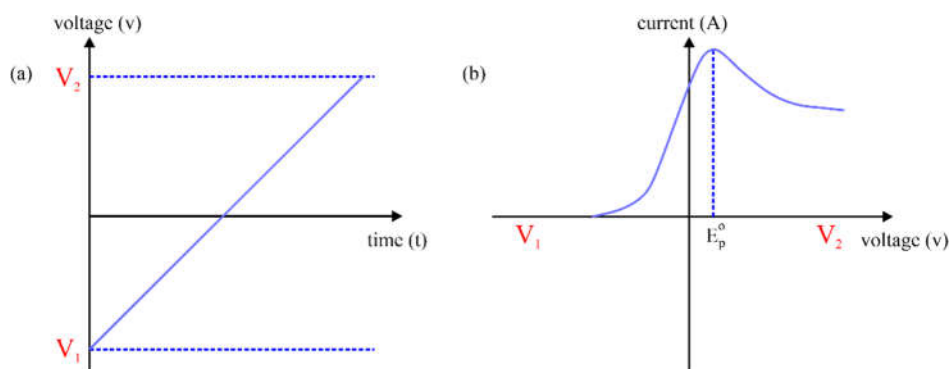


Figure 2.11 Potential changes (a) different scan rate applied and (b) graph view potential against time (Rajendrachari 2018).

As illustrated in Figure 2.11, the scan begins on the left side of the I-V plot, where no current passes. When the voltage is swept further to the right (to more reductive values), the current begins to flow and eventually reaches a peak before decreasing. The influence of the potential on the equilibrium achieved at the electrode surface is responsible for this trend. For example, the electron transfer rate is quicker

than the voltage sweep rate in the electrochemical reduction of Iron III ( $\text{Fe}^{3+}$ ) to Iron II ( $\text{Fe}^{2+}$ ). As a result, a steady state is achieved at the electrode surface that is identical to the thermodynamic predicted by the Nernst equation.

$$E = E^{\circ} + \frac{RT}{nF} \ln \frac{[\text{Fe}^{3+}]}{[\text{Fe}^{2+}]} \quad (2.1)$$

This model can predict the relationship between concentration and voltage (potential difference), where  $E$  represents the applied potential difference, and  $E^{\circ}$  represents the standard electrode potential. As the voltage is shifted from  $V_1$  to  $V_2$ , the equilibrium position of the reactant at the electrode surface shifts from no conversion at  $V_1$  to full conversion at  $V_2$ . The voltage and mass transport effects can be used to rationalise the exact form of the voltammogram.

### 2.3.1(d)(ii) Cyclic Voltammetry

CV is a very adaptable electroanalytical approach for analysing electroactive species. Due to its versatility and ease of measurement, CV is commonly employed in electrochemistry. Cyclic voltammetry is widely employed as a preliminary test in an electrochemical investigation of a substance, a biological material, or an electrode surface (Kissinger and Heineman 1983). CV's effectiveness stems from its ability to observe redox behaviour across a wide potential range rapidly. The voltammogram that results is similar to a traditional spectrum in that it conveys information as a function of an energy scan. The Cyclic voltammetry measurement technique often refers to reversing the sweep direction after each sweep of the potential has been completed to continue the sweep and repeat the reverse. As shown in Figure 2.12, the voltage-current curve (voltammogram) is commonly displayed as a result of combining two time-varying parameters (current, potential) (Gosser 1993).

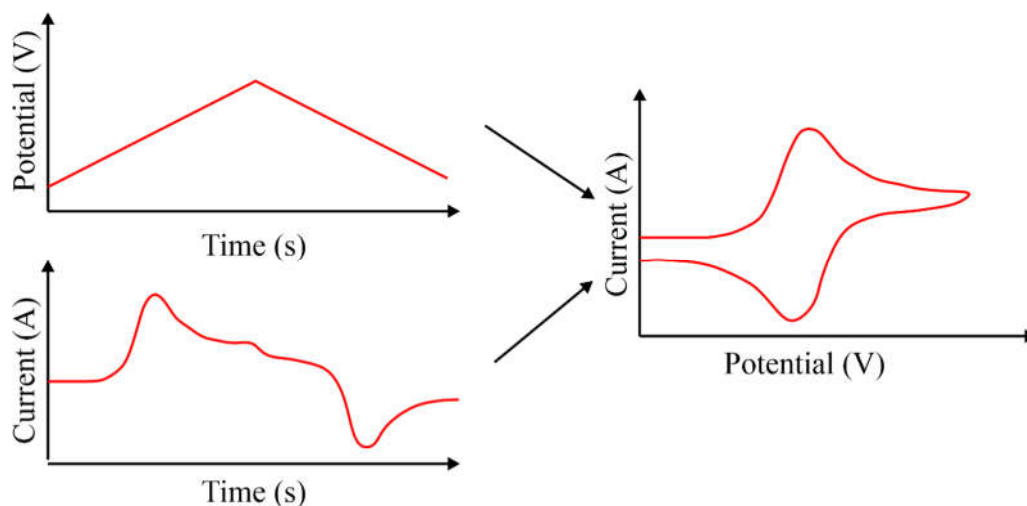


Figure 2.12 Potential wave with time changes (a); current response time (b) and (c) current vs potential (Gosser 1993).

CV involves cycling the potential of an electrode immersed in an electrolyte and measuring the current. A reference electrode, such as a saturated calomel electrode (SCE) or a silver/silver chloride electrode (Ag/AgCl), is used to control the potential of this working electrode. The excitation signal is the controlling potential applied across these two electrodes. Figure 2.13 (a) shows the CV excitation signal, a potential linear scan with a triangular waveform. The electrode's potential is swept between two values by this triangular potential excitation signal, which is also known as the switching potential. Figure 2.13 (a) illustrates how the excitation signal causes the potential to scan from +0.80 to -0.20 V vs SCE. The scan direction is reversed, resulting in a positive scan back to the original potential +0.80 V. The scan rate is 50 mV/s, as indicated by the slope. The dashed line indicates a second cycle.